Early Detection of Glaucoma from Cropped Fundus Images Using Transfer-Learned Convolutional Neural Networks

***Abstract*—Glaucoma, a leading cause of irreversible blindness, necessitates early detection for effective management. In this work, we use deep learning techniques to automate the diagnosis of glaucoma from retinal fundus images. For increased efficiency, we use a cropped fundus images instead of analyzing entire fundus photos. We use VGG-19, ResNet-50, and EfficientNet B3 for binary classification on the ACRIMA dataset. Notably, ResNet-50 achieves 100% accuracy. Next, we combine glaucoma suspect samples from publicly accessible datasets with ACRIMA and DRISHTI-GS1 to create "Glaucoma suspect" class in a custom multiclass dataset. Using this dataset, EfficientNet-B3 and ResNet-50 produce 97% and 98% accuracy rates, respectively. Both models perform flawlessly when it comes to categorizing the suspect class. Our results highlight the effectiveness of deep learning in glaucoma detection and provide interesting directions for enhancing diagnostic precision and facilitating early intervention.**

***Index Terms*—Glaucoma, Early detection, Cropped, Fundus, Transfer learning**

I. Introduction

Glaucoma is among the leading causes of irreversible blindness, making it a major public health concern.The global cumulative cases are projected to reach 111.8 million by 2040 [22]. The ocular condition is characterized by a progressive loss of the optic nerve with or without associated elevation in intraocular pressure and stereotypical changes in the cup-to-disk ratio. While the condition is typically indolent, its consequences may be catastrophic, as retinal ganglion cell damage eventually proves irreversible. About 64.3 million persons worldwide suffer from glaucoma; the incidence of true glaucoma is estimated to be 3.5% among those over 45 [21]. Glaucoma is the second most prevalent cause of visual impairment worldwide, and early detection is crucial to prevent irreversible vision loss and structural damage [23]. Automated methods for detecting glaucoma play a pivotal role in ensuring early diagnosis, particularly considering the irreversible nature of the condition once symptoms become apparent. Traditional diagnostic approaches, reliant on manual assessment by ophthalmologists, are not only labor-intensive but also subjective, leading to discrepancies among observers. Consequently, there is an urgent demand for AI-driven methodologies to streamline the diagnostic process and enhance its accuracy. By automating the diagnosis, not only is accuracy improved, but screening procedures are also expedited, allowing for timely intervention.

The integration of automated techniques into clinical practice not only optimizes resource allocation but also extends the benefits to a broader population. Our research focuses on addressing these critical healthcare needs through the development of automatic and early detection methods for glaucoma.

II. Related works

The literature review underscores glaucoma's impact on vision and surveys machine learning and deep learning in its automated diagnosis. Research shows different methods for automated glaucoma detection with different datasets and techniques. While some papers focus solely on machine learning, deep learning predominates in the majority, often in combination with other techniques.

Using a novel dataset, Islam et al. (2022) [24] suggested an automated classification strategy that makes use of deep learning models, yielding excellent accuracy. Kurilová et al. (2023) [2] investigated the use of ensemble learning methodologies and single CNN models for glaucoma detection, highlighting the efficacy of group approaches. A public dataset for glaucoma pattern recognition was presented by Bragança et al. (2022) [3], who demonstrated encouraging outcomes using deep learning frameworks. Tekouabou et al. (2021) [4] highlighted the potential of ensemble classifiers by presenting a three-step classification strategy for early glaucoma identification. Using pre-trained CNNs, Velpula and Sharma (2023) [5] present an automated glaucoma classification model. They validate it on four datasets, highlighting its potential for early glaucoma detection. Key contributions include a three-class classification framework, classifier fusion, and thorough validation. An automated glaucoma diagnostic system using HOS cumulants retrieved from RT on fundus pictures is proposed by Noronha et al. (2014) [1]. Classifying into normal, mild, and moderate/severe glaucoma, they achieve an average accuracy of 84.72% for early detection and 92.65% accuracy for all classes using NB classifier. The system shows promise for mass glaucoma screening.

Elangovan et al. (2022) [6] used the strengths of various CNN architectures to propose a deep ensemble model for glaucoma detection. Using pre-trained CNNs, Deepa et al. (2022) [7] presented a comprehensive learning system for glaucoma identification that outperformed individual models. In order to achieve excellent accuracy and recall rates in automated glaucoma diagnosis, Mahdi et al. (2022) [8] proposed an architecture based on CNN. A deep learning ensemble approach was presented by Cho et al. (2021) [9] for glaucoma

severity grading, which outperformed single CNN models in classification accuracy. All things considered, Deep learning algorithms offer promise in automating glaucoma diagnosis.

III. Methods

Here is the methodology flowchart of our work.

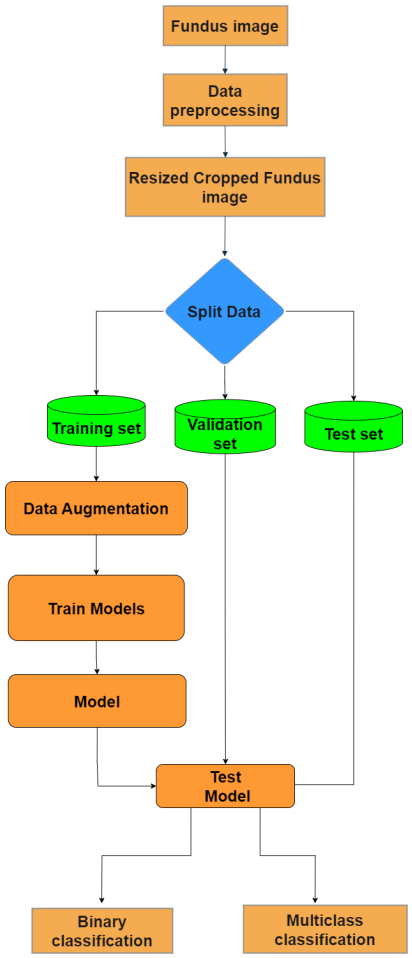

Fig. 1: Proposed Methodology

A. Dataset Description

In our study, we conducted both binary and multiclass classification tasks. For binary classification, we utilized the ACRIMA [14] dataset, comprising 326 glaucomatous samples and 239 non-glaucomatous samples.

For multiclass classification, we employed a custom dataset with three distinct labels: Glaucoma, Non-glaucoma, and Glaucoma suspect. This dataset was created by amalgamating binary labeled samples from the ACRIMA and DRISHTI-GS1 [10] datasets, along with 133 samples labeled as 'Glaucoma suspect' sourced from five additional datasets. Specifically, the ACRIMA dataset contributed 326 Glaucoma and 239 non-glaucoma samples, while the DRISHTI-GS1 dataset added 70 Glaucoma and 31 non-glaucoma samples.

Additionally, we collected 133 'Glaucoma suspect' samples from various datasets: 68 from Papila [11], 13 from JSIEC-1000 [12], 18 from OIA-ODIR [13] TRAIN, 25 from OIA-ODIR TEST-ONLINE, and 9 from OIA-ODIR TEST-OFFLINE. These samples were sourced from the SMDG-19 dataset [15] collection, available on Kaggle. So in total, 799 samples including 396 Glaucomaic, 270 Non-glaucomatic and 133 Suspect samples.

B. Data Preprocessing

Retinal fundus image preprocessing involved several steps to align with the requirements of selected pre-trained deep learning models. Initially, full fundus images were manually cropped using the 'Pinetools' online tool to isolate the optic disk and cup region. Subsequently, the cropped images were resized to dimensions compatible with the input size of the chosen pre-trained models, typically 300×300 or 224×224 pixels. A significant portion of the samples was sourced from a dataset collection named SMDG-19, already preprocessed and standardized, thereby significantly reducing the preprocessing workload.

The resizing process mathematically can be represented as follows:

1) I_{orig} denotes the original fundus image with dimensions $W_{\text{orig}} \times H_{\text{orig}}$.
2) After cropping, I_{crop} with dimensions $W_{\text{crop}} \times H_{\text{crop}}$ is obtained.
3) I_{crop} is resized to desired dimensions $W_{\text{resize}} \times H_{\text{resize}}$ using bilinear interpolation.

The resizing operation is given by:

$$I_{\text{resized}} = \text{resize}(I_{\text{crop}}, (W_{\text{resize}}, H_{\text{resize}})) \tag{1}$$

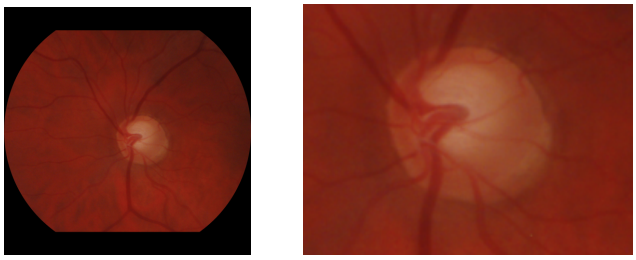

(a) Full fundus image (b) Cropped fundus image

Fig. 2: Fundus image preprocessing

These procedures guarantee that fundus images are ready for the next stage of feature extraction and deep learning model classification.

C. Data Augmentation

After splitting the dataset into training, validation, and test sets with a ratio of 80:10:10 for multiclass classification and 80:20 for binary classification (where the test and validation sets are the same), we augmented the training set. In total, we utilized 3000 images after augmentation, with 1000 images per class for multiclass classification and 2000 total training images for binary classification, maintaining a balance of 1000 images per class. The primary objective of augmentation was

to address class imbalance, which was prevalent in our dataset. Here are some of the techniques we used for augmentation:

TABLE I: Augmentation Techniques and Parameter Values

Augmentation Technique	Parameter Value
Rotation	$\pm 10^{\circ}$
Width Shift	0.1
Height Shift	0.1
Shear	0.15
Zoom	0.1
Channel Shift	10.
Horizontal Flip	True

D. Setting the Models

We have used transfer learning throughout our work. All these models were trained on the ImageNet database [16]. In total, we trained 3 different pre-trained models. VGG-19 [17], ResNet-50 [18] & EfficientNet-B3 [19] were trained for binary classification. ResNet-50, EfficientNet-B3 was trained for multiclass classification.

At first, we load the pre-trained model with pre-trained weights from ImageNet and then freeze the last layer. To generate extra parameters from our dataset, we build a custom head. It varies from model to model. We used a Global Average Pooling Layer followed by a dense layer with a 'ReLu' activation function. The Global Average Pooling (GAP) layer is a technique used in convolutional neural networks (CNNs) to reduce the spatial dimensions of feature maps while retaining important information. Mathematically, the output of the GAP layer can be computed as follows:

$$\text{GAP}(X_{ijc}) = \frac{1}{H \times W} \sum_{i=1}^{H} \sum_{j=1}^{W} X_{ijc} \tag{2}$$

We employed the same Dropout of 0.5, followed by a dense layer of 1 unit, and a 'sigmoid' activation function in all three of the binary classification models.

We first employed a global average pooling layer in multiclass classification, followed by a dense layer using the 'ReLu' activation function. With many classes to be classified, the next dense layer is composed of three units with a 'softmax' activation function. Overfitting was the main issue for the training model on that dataset as it is more diverse. So we used L2 regularization with a factor of 0.01 in both dense layers. The regularization term is a function of the weights' squared magnitude.

$$\text{L2\_regularization\_term} = \lambda \sum_{i=1}^{n} w_i^2 \tag{3}$$

where:

- λ is the regularization parameter, controlling the strength of regularization.
- w_i represents the weights in the model.
- n is the total number of weights in the model.

We used dynamic learning rate, which was defined by a custom function function consisting of some conditional statements. 'Adam' was the optimizer used to compile the model. Because of its processing efficiency, we chose it. We only trained the custom head, so the initial layers of those models were set to non-trainable. For binary classification, we employed "Binary Cross-Entropy (BCE)" as the loss function, while for multiclass classification, we utilized "Categorical Cross-Entropy (CCE)".

The binary cross-entropy loss function is defined as:

$$\text{BCE} = -\frac{1}{N} \sum_{i=1}^{N} \left(y_i \cdot \log(p_i) + (1 - y_i) \cdot \log(1 - p_i) \right) \tag{4}$$

The categorical cross-entropy loss function is defined as:

$$\text{CCE} = -\frac{1}{N} \sum_{i=1}^{N} \sum_{j=1}^{C} y_{ij} \cdot \log(p_{ij}) \tag{5}$$

We used several metrics to monitor during training. Accuracy, AUC, precision, recall, specificity and sensitivity. During training, we evaluated 'validation loss' as the core parameter.

E. Hyperparameters Settings

We evaluated different kinds of hyperparameter settings to properly fit the model. In all cases, we used 256 dense units. In the case of binary classification, the batch size is 64 and in the multiclass classification, we used a batch size of 32. Another important hyperparameter is the learning rate. We used different learning rate schedules for every model as per the model's accuracy and loss curve. Most of the time we used a decay in learning rate as the epoch goes on. We implemented the early stopping, model checkpoint, ReduceLROnPlateau in the case of multiclass classification. Regularization and early stopping helped greatly to avoid overfitting in model training.

F. Training of the Models

We set the initial epoch number as 200 in the case of multiclass but for binary classification, it was less than 30 epochs. The metric we aimed to optimize throughout the training was the validation loss, which serves as a crucial indicator of model performance and generalization ability. By monitoring validation loss, we ensured that the models were not overfitting to the training data and were capable of effectively capturing relevant patterns in the dataset.

IV. Results

A. Binary Classification

In Binary classification we trained 3 pre-trained model named VGG-19, EfficientNet-B3, ResNet-50. Table 2 elaborates the best result for each models.

TABLE II: Performance Metrics of Various Models

Models	Accuracy	F1 Score	Precision	Sensitivity
EfficientB-3	0.99	0.99	1.00	0.99
Resnet-50	1.00	1.00	1.00	1.00
VGG-19	0.95	0.95	0.94	0.96

The rigorous analysis of model performance sheds light on their effectiveness, aiding in informed decision-making

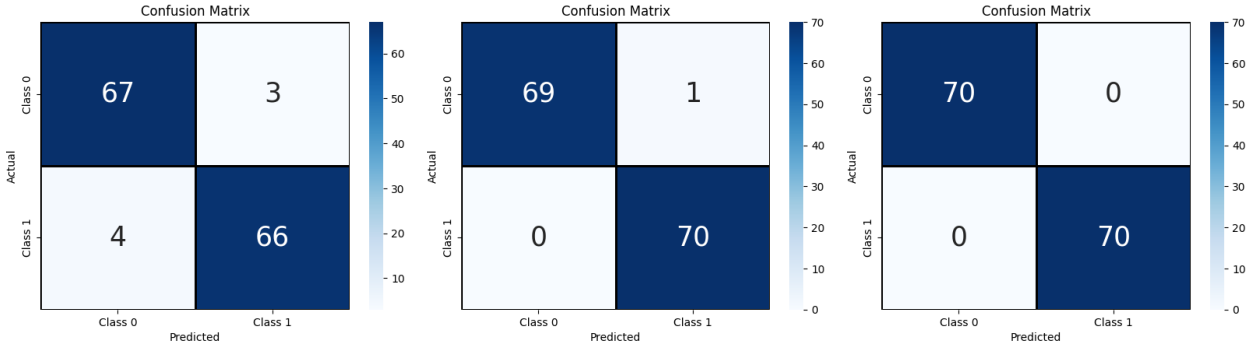

(a) Confusion Matrix for VGG-19 (b) Confusion Matrix for EfficientNet-B3 (c) Confusion Matrix for ResNet-50

Fig. 3: Confusion Matrices for Various Models

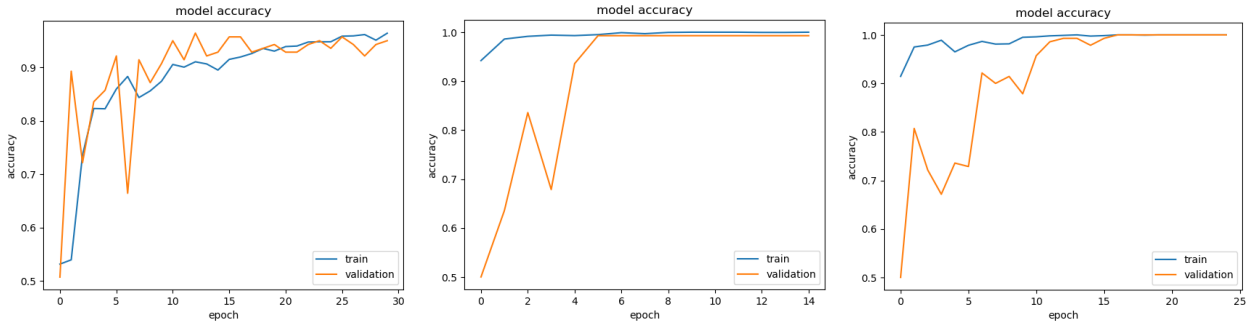

(a) Accuracy curve for VGG-19 (b) Accuracy curve for EfficientNet-B3 (c) Accuracy curve for ResNet-50

Fig. 4: Accuracy curve for Various Models(Binary classification)

for future endeavors in image classification. EfficientNet-B3 exhibited outstanding performance, boasting a remarkable accuracy of 99% and an F1 score of 99%. With a precision of 100% and a sensitivity of 99%, the model showcased excellent predictive capability. It employed standard configurations, including a gradual learning rate schedule and dropout regularization, and underwent training for 15 epochs. ResNet-50 demonstrated impeccable performance, achieving a flawless accuracy of 100% and an F1 score of 100%. With perfect precision and sensitivity metrics, both at 100%, the model showcased exemplary classification prowess. Similar to EfficientNet-B3, it adhered to a standard learning rate schedule and employed dropout regularization, undergoing training for 25 epochs. VGG-19 displayed commendable performance, attaining a respectable accuracy of 95% and an F1 score of 95%. While precision slightly trailed at 94%, sensitivity remained relatively high at 96%. Employing a similar learning rate schedule and dropout regularization, the model underwent training for 30 epochs.

In conclusion, the performance of all models showcased remarkable results, with ResNet-50 emerging as the undisputed leader, closely trailed by EfficientNet-B3. Despite its marginally lower scores, VGG-19 still showcased commendable performance, reaffirming the effectiveness of deep learning architectures in the realm of image classification tasks.

B. Multiclass Classification

In Multiclass classification, we trained ResNet-50 and EfficientNet B3 using a custom dataset. Due to limited publicly available suspect samples in a single dataset, we gathered samples from multiple sources. Suspect samples were taken from five distinct datasets and combined with the DRISHTI-GS1 dataset from ACRIMA.

TABLE III: Accuracy Comparison of EfficientNet-B3 and ResNet-50

Models	Accuracy
EfficientNet B-3	0.97
ResNet50	0.98

TABLE IV: Performance Metrics of Glaucoma Detection Models

Model	Metrics	Positive	Negative	Suspect
EfficientNet-B3	Precision	1.00	0.93	1.00
	Sensitivity	0.92	1.00	1.00
	F1 Score	0.96	0.97	1.00
ResNet-50	Precision	1.00	0.96	1.00
	Sensitivity	0.95	1.00	1.00
	F1 Score	0.97	0.98	1.00

EfficientNet-B3 impressively classifies glaucoma cases with 97% accuracy. Its flawless precision in identifying glaucoma

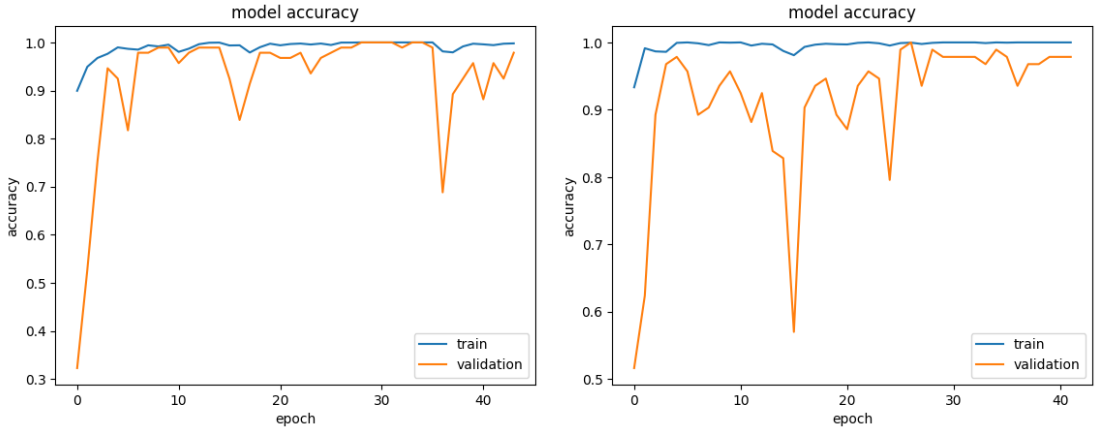

(a) Accuracy curve for EfficientNet-B3 (b) Accuracy curve for ResNet-50

Fig. 5: Accuracy curves for Various Models

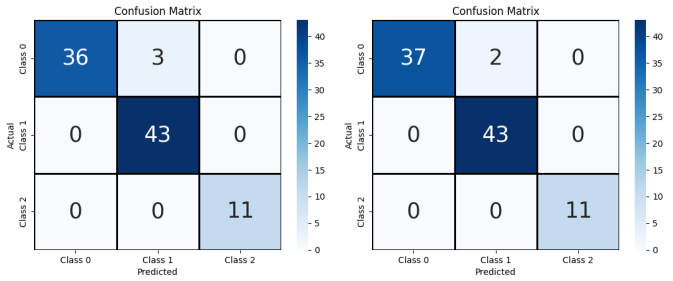

(a) For EfficientNet-B3 (b) For ResNet-50

Fig. 6: Confusion Matrices for Various Models

and suspect cases minimizes false positives. Despite slightly lower sensitivity for glaucoma cases, it maintains perfect sensitivity for non-glaucoma and suspect instances. High F1 scores across all classes showcase a balanced approach between precision and sensitivity. Training involves a dynamic learning rate schedule over 200 epochs with a batch size of 32, utilizing callbacks like EarlyStopping and ModelCheckpoint. The model's training concludes at the 44th epoch, with the best model achieved at epoch 29.

ResNet-50 outperforms EfficientNet-B3 with a 98% accuracy. It exhibits perfect precision and sensitivity across all classes, ensuring precise classification and effective identification of positive instances. High F1 scores highlight its robust performance in glaucoma detection. L2 regularization, dynamic learning rate scheduling, and Adam optimizer contribute to its training settings. Trained over 200 epochs with a batch size of 32, ResNet-50 utilizes similar callbacks, stopping at the 42nd epoch, with the best model achieved at epoch 27.

In comparison, ResNet-50 shows slightly higher accuracy than EfficientNet-B3. However, both models achieve comparable performance metrics, with negligible differences in precision, sensitivity, and F1 scores. The choice between the two may depend on specific requirements, such as computational efficiency or model interpretability. Nevertheless, meticulously designed training settings and effective callbacks significantly contribute to both models' remarkable performance in glaucoma detection.

V. Comparision with other works

Both binary & multiclass classification was intoduced in our work. Here in a table we compared our work with some other related works on the same topic.

TABLE V: A Comparition with different works

Authors	**Datasets**	**Models used**	**Best results**
Islam et al. [24]	ACRIMA (two class)	EfficientNet-B3	Acc:99%
Proposed work	ACRIMA (two class)	VGG-19, ResNet-50, EfficientNet-B3	Acc:95%, **Acc:100%** , Acc:99%
Noronha et al. [1]	Private(three class)	SVM, NB	Acc:92.65%;
Vijaya et al. [5]	Relabelled Dhrishti-gs1(three class)	Combining ResNet-50, AlexNet, VGG-19	Acc:90.55%;
Proposed work	Custom Dataset (three class)	EfficientNet-B3, ResNet-50	Acc:97%, **Acc:98%**

VI. Conclusion & Future work

In our study, our primary emphasis lay on the early identification of glaucoma. To facilitate this, we meticulously assembled a multiclass custom dataset, amalgamating various publicly accessible datasets. The introduction of the 'Glaucoma Suspect' class served as a pivotal indicator for early detection endeavors. Furthermore, we undertook binary classification alongside. Across both classification scenarios, we deployed multiple pre-trained models. Notably, in both contexts, ResNet-50 emerged as the top performer, achieving a remarkable 100% accuracy in binary classification and an impressive 98% accuracy in multiclass classification. Notably,

our model exhibited flawless detection of suspect class samples, thereby reinforcing its efficacy in facilitating the early identification of glaucoma.

Looking ahead, future research could focus on several areas to further enhance model performance and applicability. Firstly, incorporating additional datasets with diverse demographics and imaging conditions could improve model generalization. Fine-tuning model hyperparameters and architectures may yield even better results. Additionally, exploring the integration of multimodal data, such as combining retinal images with patient metadata or genetic information, could provide deeper insights into glaucoma diagnosis and prognosis. Furthermore, deploying trained models in real-world clinical settings and conducting prospective studies to evaluate their performance and impact on patient outcomes would validate their utility in clinical practice. Continued research in this direction holds promise for advancing automated glaucoma diagnosis and improving patient care.

REFERENCES

[1] Noronha, K. P., Acharya, U. R., Nayak, K. P., Martis, R. J., & Bhandary, S. V. (2014, March). Automated classification of glaucoma stages using higher order cumulant features. Biomedical Signal Processing and Control, 10, 174–183. https://doi.org/10.1016/j.bspc.2013.11.006

[2] V. Kurilová, S. Rajcsányi, Z. Rábeková, J. Pavlovičová, M. Oravec, and N. Majtánová, "Detecting glaucoma from fundus images using ensemble learning," Journal of Electrical Engineering, vol. 74, p. 328–335, Aug 2023.

[3] C. P. Bragança, J. M. Torres, C. P. Soares, and L. O. Macedo, "Detection of glaucoma on fundus images using deep learning on a new image set obtained with a smartphone and handheld ophthalmoscope," Healthcare, vol. 10, p. 2345, Nov 2022.

[4] C. S. Koumetio Tekouabou, E. A. ABDELLAOUI ALAOUI, I. Chabbar, W. Cherif, and S. Hassan, "Using deep features extraction and ensemble classifiers to detect glaucoma from fundus images," pp. 63–70, 01 2021

[5] Velpula, V. K., & Sharma, L. D. (2023, June 13). Multi-stage glaucoma classification using pre-trained convolutional neural networks and voting-based classifier fusion. Frontiers in Physiology, 14. https://doi.org/10.3389/fphys.2023.1175881.

[6] P. Elangovan and M. K. Nath, "enconvnet: A novel approach for glaucoma detection from color fundus images using ensemble of deep convolutional neural networks," Inter- national Journal of Imaging Systems and Technology, vol. 32, p. 2034–2048, May 2022.

[7] N. Deepa, S. Esakkirajan, B. Keerthiveena, and S. B. Dhanalakshmi, "Automatic diagno- sis of glaucoma using ensemble based deep learning model," vol. 1, pp. 536–541, 2021.

[8] M. M. Mahdi, M. A. Mohammed, H. Al-Chalibi, B. S. Bashar, H. A. Sadeq, and T. M. J. Abbas, "An ensemble learning approach for glaucoma detection in retinal images," Dec 2022.

[9] H. Cho, Y. H. Hwang, J. K. Chung, K. B. Lee, J. S. Park, H.-G. Kim, and J. H. Jeong, "Deep learning ensemble method for classifying glaucoma stages using fundus photographs and convolutional neural networks," Current Eye Research, vol. 46, p. 1516–1524, Apr 2021.

[10] Sivaswamy, Jayanthi, S. R. Krishnadas, G. Ramakrishna Dutt, Joshi, Madhulika Jain, Ujjwal Syed and Tabish A. "Drishti-GS: Retinal image dataset for optic nerve head(ONH) segmentation." 2014 IEEE 11th International Symposium on Biomedical Imaging (ISBI) (2014): 53-56.

[11] O. Kovalyk, J. Morales-Sánchez, R. Verdú-Monedero, I. Sellés-Navarro, A. Palazón- Cabanes, and J.-L. Sancho-Gómez, "Papila: Dataset with fundus images and clinical data of both eyes of the same patient for glaucoma assessment," Scientific Data, vol. 9, no. 1, p. 291, 2022.

[12] Cen, LP., Ji, J., Lin, JW. et al. Automatic detection of 39 fundus diseases and conditions in retinal photographs using deep neural networks. Nat Commun 12, 4828 (2021). https://doi.org/10.1038/s41467-021-25138-w

[13] Li, N., Li, T., Hu, C., Wang, K., Kang, H. (2021). A Benchmark of Ocular Disease Intelligent Recognition: One Shot for Multi-disease Detection. In: Wolf, F., Gao, W. (eds) Benchmarking, Measuring, and Optimizing. Bench 2020. Lecture Notes in Computer Science(), vol 12614. Springer, Cham.https://doi.org/10.1007/978-3-030-71058-3_11

[14] A. Diaz-Pinto, S. Morales, V. Naranjo, T. Kohler, J. M. Mossi, and A. Navea, "Cnns for automatic glaucoma assessment using fundus images: an extensive validation," Biomedical engineering online, vol. 18, no. 1, pp. 1–19, 2019.

[15] Riley Kiefer, Muhammad Abid, Jessica Steen, Mahsa Raeisi Ardali, and Ehsan Amjadian. 2023. A Catalog of Public Glaucoma Datasets for Machine Learning Applications: A detailed description and analysis of public glaucoma datasets available to machine learning engineers tackling glaucoma-related problems using retinal fundus images and OCT images. In Proceedings of the 2023 7th International Conference on Information System and Data Mining (ICISDM '23). Association for Computing Machinery, New York, NY, USA, 24–31. https://doi.org/10.1145/3603765.3603779

[16] J. Deng, W. Dong, R. Socher, L. -J. Li, Kai Li and Li Fei-Fei, "ImageNet: A large-scale hierarchical image database," 2009 IEEE Conference on Computer Vision and Pattern Recognition, Miami, FL, USA, 2009, pp. 248-255, doi: 10.1109/CVPR.2009.5206848. keywords: Large-scale systems;Image databases;Explosions;Internet;Robustness;Information retrieval;Image retrieval;Multimedia databases;Ontologies;Spine.

[17] Simonyan, Karen & Zisserman, Andrew. (2014). Very Deep Convolutional Networks for Large-Scale Image Recognition. arXiv 1409.1556.

[18] K. He, X. Zhang, S. Ren and J. Sun, "Deep Residual Learning for Image Recognition," 2016 IEEE Conference on Computer Vision and Pattern Recognition (CVPR), Las Vegas, NV, USA, 2016, pp. 770-778, doi: 10.1109/CVPR.2016.90. keywords: Training;Degradation;Complexity theory;Image recognition;Neural networks;Visualization;Image segmentation.

[19] Mingxing Tan, Quoc V. Le. "EfficientNet: Rethinking Model Scaling for Convolutional Neural Networks." arXiv preprint arXiv:1905.11946 (2020).

[20] R. Janani, S.P. Rajamohana, Early detection of glaucoma using optic disc and optic cup segmentation: A survey, Materials Today: Proceedings, Volume 45, Part 2, 2021, Pages 2763-2769, ISSN 2214-7853, https://doi.org/10.1016/j.matpr.2020.11.613. (https://www.sciencedirect.com/science/article/pii/S2214785320392877)

[21] Zedan, Mohammad & Zulkifley, Mohd Asyraf & Ibrahim, Ahmad & M Moubark, Asraf & Mohamed Kamari, Nor Azwan & Abdani, Siti Raihanah. (2023). Automated Glaucoma Screening and Diagnosis Based on Retinal Fundus Images Using Deep Learning Approaches: A Comprehensive Review. Diagnostics. 13. 2180. 10.3390/diagnostics13132180. 0.

[22] Quigley HA, Broman ATThe number of people with glaucoma worldwide in 2010 and 2020British Journal of Ophthalmology 2006;90:262-267.

[23] Quigley, H.A. and Broman, A.T., 2006. The number of people with glaucoma worldwide in 2010 and 2020. British journal of ophthalmology, 90(3), pp.262-267.

[24] Islam, M. T., Mashfu, S. T., Faisal, A., Siam, S. C., Naheen, I. T., & Khan, R. (2022). Deep Learning-Based Glaucoma Detection With Cropped Optic Cup and Disc and Blood Vessel Segmentation. IEEE Access, 10, 2828–2841. https://doi.org/10.1109/access.2021.3139160